

Quantized shift response in multi-gap topological phases

Wojciech J. Jankowski^{1,*} and Robert-Jan Slager^{1,†}

¹*TCM Group, Cavendish Laboratory, Department of Physics,
J J Thomson Avenue, Cambridge CB3 0HE, United Kingdom*

(Dated: February 21, 2024)

We show that certain 3D multi-gap topological insulators can host quantized shift photoconductivities due to bulk invariants that are defined under reality conditions imposed by additional symmetries. We recast the quantization in terms of the integrated torsion tensor and the non-Abelian Berry connection constituting Chern-Simons forms. Physically, we recognize that the topological quantization emerges purely from virtual transitions contributing to the optical response. Our findings provide another quantized electromagnetic DC response due to the non-trivial band topology, beyond the quantum anomalous Hall effect of Chern insulators and quantized circular photogalvanic effect found in Weyl semimetals.

Introduction.— Topological insulators and semimetals constitute an active research area in condensed matter physics [1–4]. Amid a fast track of progress, especially the past years have seen the emergence of a rather uniform view on a large fraction of topological materials upon including crystalline symmetries [5–10]. In particular, considering how irreducible representations at high symmetry points need to consistently glue together over the whole Brillouin zone, one may obtain a set of exhaustive consistency equations [7] that upon comparing to real space Wannierization conditions leverages universally implementable schemes to discern topological materials [8, 10].

More recently, however, further advances have revealed a new class of topological phases that depend on multi-gap conditions [11–15] and cannot be a priori captured by symmetry-indicated methods. In such phases, band spaces can acquire novel multi-gap invariants. In particular, in presence of a reality condition of the Hamiltonian, such as the presence of $\mathcal{C}_2\mathcal{T}$ (two-fold rotations and time reversal) or \mathcal{PT} (parity and time reversal) symmetries, band degeneracies can carry non-Abelian charges [16], akin to disclination charges in a bi-axial nematic [17–20]. As a result of braiding processes, band subspaces can subsequently come to host a set of similarly-valued charges that can not be removed, posing an obstruction to annihilate as long as the gaps with the other parts of spectrum are maintained [12, 21]. This obstruction to annihilate degeneracies within the band subspace is moreover quantified by a topological invariant, the Euler class [11, 12, 22].

While the multi-gap point of view opens up novel theoretical pursuits, including deeper relations with homotopy theory [11], recent developments have shown distinctive physical signatures of these kinds of phases [23]. In the out-of-equilibrium context, novel Floquet phases were postulated [24] and monopole–anti-monopole creation in the quench dynamics of Euler phases captured

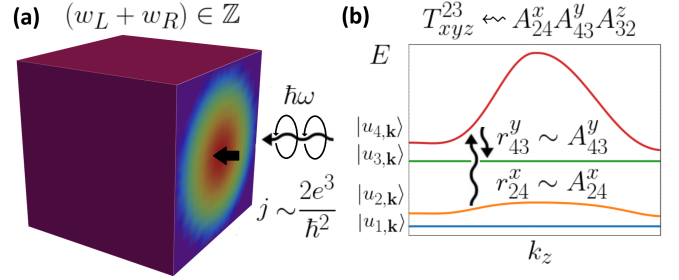


FIG. 1. (a) Quantized bulk photovoltaic shift currents induced by incident light. A second-order DC current density response $j_z(0)$ of a multi-gap non-Abelian topological insulator with photoconductivity quantized in terms of $2\frac{e^3}{\hbar^2}$, on coupling circularly-polarized light with photon energy $\hbar\omega$ and electric field $\mathcal{E}(\frac{x+iy}{\sqrt{2}})$. The shift response is due to virtual transitions, as captured by the torsion tensor T_{abc}^{nm} between the occupied and unoccupied bands. (b) Diagrammatic representation of the corresponding virtual transitions between topological bands, inducing a shift response encoded by the torsion tensor. Transition dipole amplitudes r_{24}^x, r_{43}^y from band $|u_{2,k}\rangle$ to $|u_{3,k}\rangle$, virtually through $|u_{4,k}\rangle$, are indicated. These are proportional to the elements of non-Abelian Berry connection A_{24}^x, A_{43}^y , contributing to the torsion tensor element T_{xyz}^{23} .

by a Hopf map was predicted [25]. The latter was in fact recently observed [26]. Similarly, stress or strain has been predicted to lead to braiding and Euler invariants in the context of phononic [27, 28] and electronic spectra [12, 29] of real materials, where in the electronic case it was also shown that multi-gap physics can arise by virtue of structural phase transitions [30]. Finally, multi-gap topologies are increasingly finding their way to metamaterial experiments [31–35].

A hallmark of topological materials is that they can render quantized responses. Chern bands for example were shown to exhibit quantized anomalous Hall (QAH) and quantized dichroism responses [36–39]. Similarly, Weyl semimetals can be probed by second-order quantized circular photogalvanic effects (QCPGE) [40–43]. We note that these phenomena are presently more and

* wjj25@cam.ac.uk

† rjs269@cam.ac.uk

more understood from the upcoming perspective of quantum geometry. Following formulations of quantum geometric tensors (QGT) quite some time ago [44, 45], these concepts have recently been reinvigorated in several contexts that range from superconductivity and superfluidity to transport properties [46–49]. Response theories fit particularly well in this context [50] as they relate directly to elements of QGTs (see also Appendix A). Recent progress includes rephrasing matrix elements of optical processes in terms of Riemannian geometry [51], and moreover a universal strategy in terms of Plücker embeddings [52], to effectively calculate geometric entities and QGTs, and thus accordingly optical responses, in general multi-band systems.

The mentioned mathematical Plücker framework works in two directions. Apart from quantifying geometry, it allows for an efficient method to model topological phases for arbitrarily partitioned band spaces. As such, this approach has stood at the basis of generalizing multi-gap topologies to fully-generalized settings, as it allows for a direct evaluation of the classifying space set by the Hamiltonian [11, 14]. Particular examples include three dimensional (3D) phases of real-valued 4-band Hamiltonians, displaying a double Hopf invariant when the bands are partitioned in two 2-band subspaces [53], a Pontryagin index if the bands partition into a 3-band and a 1-band subspace [54], or two winding numbers relating to isoclinic rotations when all bands are non-degenerate, referred to as so-called generalized multi-gap flag phases [11, 14, 54] (for more details, see Appendix B).

It is in this field of interplay of geometrical insights, non-Abelian multi-gap notions in three-dimensional systems, and non-linear optical responses, that we find our results. Namely, in this work, we discover quantized photovoltaic shift effect in three-dimensional non-Abelian topological insulators enjoying a reality condition. In particular, we show that (i) the shift response in these systems is purely governed by the virtual transitions in the topological multi-band subspaces, which (ii) we identify with the non-triviality of the torsion tensor introduced in the Riemannian-geometric reformulation of the optical responses [51]. Correspondingly, we retrieve its quantization from the real Chern-Simons forms (iii), directly related to the aforementioned Hopf indices. We numerically validate these findings in the minimal models capturing the relevant non-Abelian topologies (iv). In this context, we identify (v) the *quantized changes* of the shift response induced by the virtual transitions over topological phase transitions (TPTs). Finally, we discuss the novel *quantized* shift effect, and its changes across TPTs, in the context of candidate materials.

Non-linear optical shift responses.— The non-linear second-order optical shift responses central to this work are manifested by bulk DC photovoltaic currents,

$$j_c(0) = \sum_{a,b=x,y,z} \sigma_{\text{shift}}^{cab}(\omega) \mathcal{E}_a(\omega) \mathcal{E}_b(-\omega), \quad (1)$$

induced on coupling a 3D material to AC electric

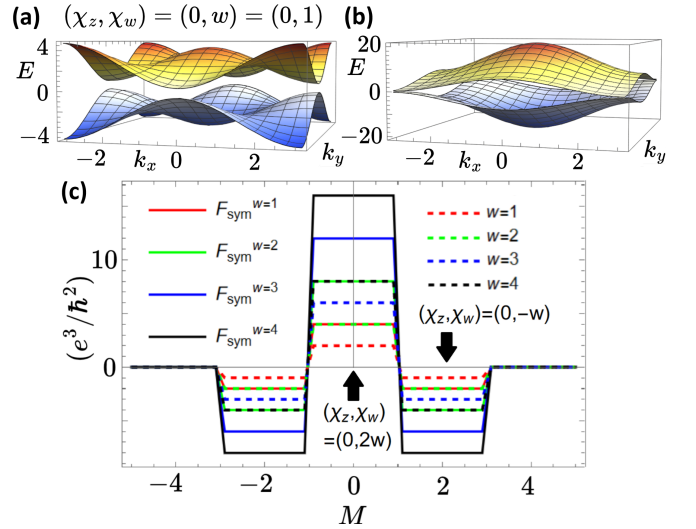


FIG. 2. (a) Topological band structure of a Real Hopf Insulator ($k_z = 0$). (b) Band structure of RHI model, Eq. (9), for $M = 3/2$, exhibiting a semimetallic node emerging at the BZ edge $(k_x, k_y, k_z) = (\pi, \pi, 0)$, across the topological phase transition. (c) The variation of the quantized shift effect represented by F_{sym} , indicating TPTs at $M = 3/2$ and $M = 3$, across which both topological bulk invariant and the associated quantized integrated shift photoconductivities F_{sym} change sharply. Namely, in the central, low $|M|$ region, $(\chi_z, \chi_w) = (0, 2w)$, and for $3/2 < |M| < 3$, $(\chi_z, \chi_w) = (0, -w)$.

field with components of magnitude $\mathcal{E}_a(\omega)$, where ω is the frequency of incident electromagnetic radiation. The second-order shift photoconductivity $\sigma_{\text{shift}}^{cab}(\omega)$, which can be decomposed in terms of linear $\sigma_{\text{shift,L}}^{cab}(\omega)$ and circular $\sigma_{\text{shift,C}}^{cab}(\omega)$ contributions picked by the corresponding light polarizations ($\sigma_{\text{shift}}^{cab}(\omega) = \sigma_{\text{shift,L}}^{cab}(\omega) + i\sigma_{\text{shift,C}}^{cab}(\omega)$) [22] was formulated in terms of the momentum-space derivatives of the QGT, encoded by a Hermitian connection C_{abc}^{mn} [51] (see also Appendix A). More explicitly, $C_{bca}^{mn} = -i r_{nm}^b r_{mn}^a R_{mn}^{c,a}$ [51, 55], in terms of the transition dipole moments $r_{nm}^a = i(1 - \delta_{mn})A_{nm}^a$, given by the non-Abelian Berry connection $A_{nm}^a = \langle u_{n,\mathbf{k}} | \partial_{k_a} u_{m,\mathbf{k}} \rangle$, with $|\psi_{n,\mathbf{k}}\rangle = e^{i\mathbf{k}\cdot\mathbf{r}} |u_{n,\mathbf{k}}\rangle$, the Bloch states. Here, $R_{mn}^{c,a} \equiv A_{mm}^c - A_{nn}^c + i\partial_{k_c} \log r_{mn}^a$ is the ‘shift vector’, associated with the name of the effect. Intuitively, $R_{mn}^{c,a}$ reflects a positional shift of an electron upon optical transition [56, 57]. In terms of C_{abc}^{mn} , the photoconductivity reads [51],

$$\sigma_{\text{shift}}^{cab}(\omega) = \frac{\pi e^3}{2\hbar^2} \sum_{m,n} \int_{\text{BZ}} \frac{d^3k}{(2\pi)^3} \delta(\omega - \omega_{mn}) f_{nm} i (C_{bca}^{nm} - C_{acb}^{mn}). \quad (2)$$

In the above, an integration of the Hermitian connection over the entire Brillouin zone (BZ) is assumed, f_{nm} are the differences in the Fermi occupation factors of correspondingly occupied and unoccupied bands n, m , which are split by energies $\hbar\omega_{mn}$. Importantly, the key ingredient of the response, C_{abc}^{mn} , defines the torsion tensor T_{abc}^{mn} ,

a quantity central to this work,

$$T_{abc}^{mn} \equiv C_{abc}^{mn} - C_{acb}^{mn}. \quad (3)$$

Following Ref. [51], we notice that physically the torsion tensor is associated with virtual transitions between three bands n, p, m (for reference, see Fig. 1). The question is, if such transitions can result in a topological quantized response in certain scenarios. In the following, we provide a positive answer.

Results.— The central result of this work is to recognize that the integrated *circular* shift photoconductivity relevant for the net bulk photovoltaic responses [58], can be expressed in terms of the torsion tensor (see Appendix C for a full derivation),

$$\begin{aligned} & \int d\omega (\sigma_{\text{shift},C}^{abc}(\omega) + \sigma_{\text{shift},C}^{bca}(\omega) + \sigma_{\text{shift},C}^{cab}(\omega)) \\ &= -\frac{e^3}{8\pi^2\hbar^2} \int_{\text{BZ}} d^3k \sum_{m,n} f_{mn} (T_{abc}^{mn} + T_{bca}^{mn} + T_{cab}^{mn}). \end{aligned} \quad (4)$$

Centrally, for non-Abelian multi-gap topological insulators as considered in this work, we recognize that it is naturally possible to induce torsion in any four real Bloch bands close to the Fermi level $\{|u_{1,\mathbf{k}}\rangle, |u_{2,\mathbf{k}}\rangle, |u_{3,\mathbf{k}}\rangle, |u_{4,\mathbf{k}}\rangle\}$. Here, two bands are occupied and two are unoccupied. Correspondingly, we provide schematics for the virtual transitions associated with the torsion in Fig. 1. Furthermore, on additionally considering the zero-temperature limit, $f_{nm} = 1$, we retrieve (see Appendix D):

$$\begin{aligned} F_{\text{sym}} &\equiv -i \int d\omega (\sigma_{\text{shift}}^{xyz}(\omega) + \sigma_{\text{shift}}^{yzx}(\omega) + \sigma_{\text{shift}}^{zxy}(\omega)) \\ &= \frac{e^3}{4\pi^2\hbar^2} \int_{\text{BZ}} d^3k (\mathbf{a}^v \cdot \mathbf{E}\mathbf{u}^v + \mathbf{a}^c \cdot \mathbf{E}\mathbf{u}^c), \end{aligned} \quad (5)$$

as $\sigma_{\text{shift},L}^{cab}(\omega) = 0$ vanishes by the reality condition. Following the notion of the ‘figure of merit’ of Ref. [58], here we spectrally integrate the shift photoconductivities to obtain a symmetrized analogue, F_{sym} . Furthermore, we define Euler connections and curvatures [12] in terms of the pairs of conduction and valence bands $\mathbf{a}^{v/c} = \langle u_{2/4,\mathbf{k}} | \nabla_{\mathbf{k}} | u_{1/3,\mathbf{k}} \rangle$, $\mathbf{E}\mathbf{u}^{v/c} = \nabla_{\mathbf{k}} \times \mathbf{a}^{v/c}$. As shown in Appendix D, the integrand can be written as the sum of Chern-Simons 3-forms, given by non-Abelian Berry connection matrices A_{nm}^a as $\text{Tr}[\epsilon_{abc}(A_{nm}^a \partial_{k_b} A_{mn}^c + \frac{2}{3} A_{nm}^a A_{mp}^b A_{pn}^c)]$, constrained under the reality condition, which provides a quantization upon integrating over the compact BZ 3-torus. Thus, we obtain a quantized second-order photovoltaic shift effect on coupling to circularly-polarized light, purely due to the virtual transitions in the real non-Abelian topological bands. We thus identify a second-order shift current cousin of the QCPGE manifested by the second-order injection currents in the Weyl semimetals [40, 59].

We recognize that the quantized response is present in the aforementioned real Hopf insulators [53] (RHIs) classified by homotopy, $\pi_3[S^2 \times S^2] \cong \mathbb{Z} \oplus \mathbb{Z} \equiv \mathbb{Z}^2$, of a

double Hopf fibration (see also Appendix B), as the integrated 3-form introduced in Eq. (5) can be recast in terms of two real Hopf invariants. The Hopf invariants χ_z, χ_w require two occupied, and unoccupied bands, which can be taken fully degenerate (see Fig. 2). In particular, these invariants can be expressed by adding/subtracting products of the Euler curvature and connection elements mixing both valence and conduction bands [53]: $\mathbf{a}^c \cdot \mathbf{E}\mathbf{u}^v$ and $\mathbf{a}^v \cdot \mathbf{E}\mathbf{u}^c$, in the integrand of Eq. (5) (see Appendix B for further details). In that case, we ultimately obtain:

$$F_{\text{sym}} = \frac{2e^3}{\hbar^2} (\chi_z + \chi_w). \quad (6)$$

Furthermore, we recognize that beyond the RHIs, the quantization condition is expected to hold in a broader class of non-Abelian topological insulators satisfying the reality condition imposed by \mathcal{PT} symmetries. In particular, this includes the recently introduced multi-gap topological phases classified by real flag manifolds ($\pi_3[\text{Fl}_{1,1,1,1}(\mathbb{R})] \cong \mathbb{Z}^2$) being isoclinic rotation winding numbers w_L, w_R . Here, all four bands are isolated by topological gaps, all admitting topological edge modes induced by the bulk invariant and π -Zak phases [54]. Analogously to the RHIs, the invariants w_L, w_R can be expressed in terms of the non-Abelian Berry connections defining Chern-Simons 3-forms of Eq. (5), see also Appendix B for more details on the classification of flag manifolds and multiply gapped non-Abelian insulators. In this case, we similarly obtain:

$$F_{\text{sym}} = \frac{2e^3}{\hbar^2} (w_L + w_R). \quad (7)$$

While w_L and w_R can be obtained analogously to the real Hopf invariants from the non-Abelian Berry connections, these are not associated with the Hopf fibrations, which characterize the mappings of two-band subbundles to 2-spheres $S^2 \times S^2$. In other words, each winding number corresponds to a non-trivial element of $\pi_3[S^3]$, rather than $\pi_3[S^2]$. In particular, the multiply-gapped flag insulators support edge states in all three topological gaps between four topological bands [54]. Finally, we retrieve a quantized response due to a single topological index, rather than two, under the $3 \oplus 1$ band partitioning of \mathcal{PT} -symmetric phases with Pontryagin index $Q \in \mathbb{Z}$ [54]; where Q corresponds to the single homotopy, $\pi_3[S^3] \cong \mathbb{Z}$ (see Appendix B). Here, to access all transitions necessary for the quantization of the response, one band below the principal gap needs to become depopulated, up to the band degeneracies between the second and third band, yielding a semimetallic state. Correspondingly, such non-Abelian semimetals enjoy a simple quantization as,

$$F_{\text{sym}} = \frac{2e^3}{\hbar^2} Q, \quad (8)$$

completing the glossary of quantized shift responses due to different types of non-Abelian four-band topologies, as identified in this work.

Model realizations.— We now concretize the above ideas in the context of simple models. For details on general classes of models capturing the considered band topologies, we furthermore refer to Appendix B.

In Fig. 2, we demonstrate the results for RHIs. Here, we present the evolution of quantized shift responses in the RHI models with $(\chi_z, \chi_w) = (0, w)$, taking the form $H(\mathbf{k}) = R_w(\mathbf{k}) \text{diag}(-1, -1, 1, 1) R_w^T(\mathbf{k})$ generated with a matrix of Bloch eigenvectors,

$$R_w(\mathbf{k}) = \sin w k_x \Gamma_{11} + i \sin k_y \Gamma_{23} - \sin k_z \Gamma_{31} + (M - \cos w k_x - \cos k_y - \cos k_z) \Gamma_{03}, \quad (9)$$

where $\Gamma_{ij} = \sigma_i \otimes \sigma_j$ are 4×4 Kronecker products of identity and Pauli matrices $(\sigma_0, \sigma_1, \sigma_2, \sigma_3) \equiv (\mathbf{1}_2, \sigma_x, \sigma_y, \sigma_z)$. Here, M is the topological mass, changes of which can cause phase transitions trivializing the RHI. In Fig. 3, we show analogous results for the multi-gap flag phases. Here, we also employ models with tunable topological mass M . In particular, we choose $H(\mathbf{k}) = V_R V_L^T \text{diag}[-2, -1, 1, 2] V_L V_R^T$ with,

$$V_{L/R} = \sin w_{L/R} k_x \Gamma_{11} + i \sin k_y \Gamma_{23} - \sin k_z \Gamma_{31} + (M - \cos w_{L/R} k_x - \cos k_y - \cos k_z) \Gamma_{03}, \quad (10)$$

in terms of the isoclinic winding numbers w_L, w_R . In both cases, we observe sharp quantized jumps in the integrated shift responses F_{sym} , coinciding with the values of topological masses corresponding to TPTs. Naturally, we expect F_{sym} to vanish, as the topological numbers dictating the optical shift response in one-to-one correspondence are trivialized. At the TPT points, the systems become metallic on gap closings, which results in crossover F_{sym} values across the jumps. Notably, the shift photoconductivities in topological semimetals, including \mathcal{PT} -symmetric models, were extensively studied in Refs. [22, 60–62].

Discussion.— Having introduced the topological quantized phenomenology of the shift responses in non-Abelian phases, we address the possibilities of observing such physical effects and how our results galvanize new areas of investigation. Firstly, similarly to the behaviour of QCPGE associated with the second-order injection (rather than shift) currents, we expect that on observing such a characteristic sharp response, the quantization of the proposed effect might be mildly violated on introducing the corrections due to the electron-electron interactions [42]. Additionally, one could also wonder about how significant a contribution to the shift currents due to the 2D surface modes correspondent to the non-trivial non-Abelian 3D topological bulk could be. Here it is important to notice that the surface bands are unlikely to contribute to F_{sym} , because by construction it necessarily involves combinations of all three spatial dimensions in each constituent photoconductivity term. Finally, it remains an open question, beyond the momentum-conserving formulation, of how robust the quantized effect is in real disorder materials, lacking translational

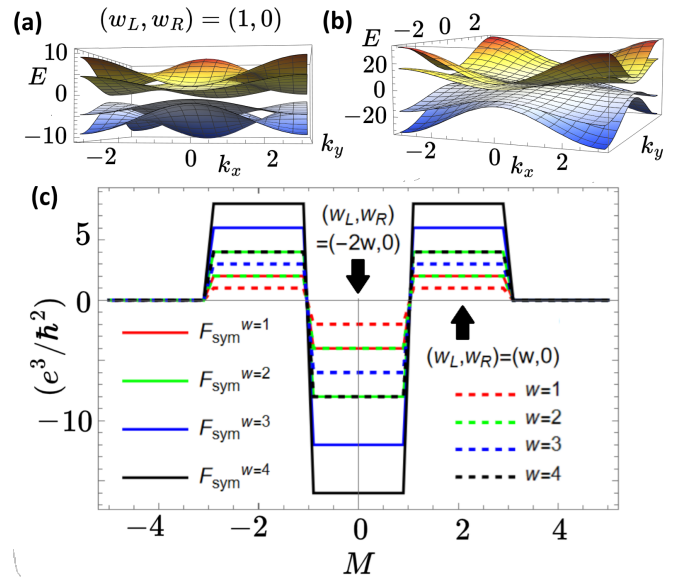


FIG. 3. (a) Topological band structure of the non-Abelian multi-gap flag phase for $k_z = \pi/2$. (b) Band structure at the critical topological mass $M = 3$ of the flag phase with a semimetallic node emerging at the BZ centre $(k_x, k_y, k_z) = (0, 0, 0)$ across the TPT. (c) The quantized shift effect represented by F_{sym} , changing sharply with the topological mass, across the values $|M| = 3/2$, $|M| = 3$. Correspondingly, the bulk topological invariant changes, and trivializes further, $(w_L, w_R) = (-2w, 0) \rightarrow (w, 0) \rightarrow (0, 0)$.

symmetries. While the aspects of disorder and interactions motivate a separate extensive study, which we leave for future, at the same time we naturally identify \mathcal{PT} -symmetric 3D topological phases, amongst the candidate materials to realize the effect. Such phases include CuMnAs, a system modelled with a four-band low-energy theory, already known to support chiral gyration photocurrents, which include j_x induced by Hermitian connection elements C_{xxy}, C_{yyx} , under circularly-polarized light [63, 64], or phases obtainable from anti-ferromagnetic $\text{MnBi}_{2n}\text{Te}_{3n+1}$ heterostructures [65–67], which were recently related to non-trivial quantum geometry [68]. In particular, a measurable quantized jump in F_{sym} is expected across TPT, if the considered multi-gap topologies were present. Importantly, to obtain the non-trivial second-order shift effect, the material needs to be non-centrosymmetric [56], i.e. break \mathcal{P} symmetry. Hence to preserve \mathcal{PT} , it also necessarily needs to break \mathcal{T} symmetry, i.e. be magnetic. Indeed, for RHI, \mathcal{P} symmetry is admitted only if $\chi_w + \chi_z = 0$ [53], which yields no shift response, consistently with Eq. (6).

We finally note that recently it was suggested that virtual transitions can constitute a significant contribution to shift currents in the multi-band systems, in particular, layered moiré materials [69], and there might exist interesting connections to the band topology. Here, we precisely retrieve such a connection, manifestly captured by a quantization encoded in the virtual multi-

band transitions. Additionally, we show that indeed, the changes in the band topology across TPTs directly result in the quantized jumps of the shift responses present in non-Abelian multi-band topological insulators. Relating the above results and multi-gap phases to moiré van der Waals platforms therefore generally entails for a promising future pursuit.

Summary and Outlook.— We identify a new *quantized* photovoltaic response in terms of (circular) shift photoconductivities manifested by associated second-order currents, which can be induced by non-trivial non-Abelian multi-gap band topology. We analytically and numerically retrieve this response in topological phases with real Hopf, flag manifold, or Pontryagin-indexed, multi-gap topology, captured by minimal four Bloch band models under reality conditions. In particular, we show that the integrated total shift effect, purely contributed by the virtual interband transitions, can indicate topological phase transitions in non-Abelian topological phases. Hence, we find another unique topological quantized DC response, beyond QAH effect in Chern insulators and QCPGE in Weyl semimetals, providing a smoking-gun criterion for the search of exotic non-Abelian multi-gap topological phases.

ACKNOWLEDGMENTS

W.J.J. acknowledges funding from the Rod Smallwood Studentship at Trinity College, Cambridge. R.-J.S. acknowledges funding from a New Investigator Award, EPSRC grant EP/W00187X/1, a EPSRC ERC underwrite grant EP/X025829/1, and a Royal Society exchange grant IES/R1/221060, as well as Trinity College, Cambridge. We cordially thank Zory Davoyan, Adrien Bouhon, and F. Nur Ünal for numerous discussions concerning non-Abelian and multi-gap topological phases. R.-J. S thanks Joel E. Moore for discussions.

Note added: While completing this manuscript, we became aware of the work [69] on enhancing shift currents via multiband transitions, although in the 2D context of moiré materials. Here, beyond retrieving an unprecedented *quantized* shift response due to the virtual transitions in 3D systems, we explicitly demonstrate shift responses for probing TPTs in 3D multiband topological materials.

-
- [1] X.-L. Qi and S.-C. Zhang, Topological insulators and superconductors, *Rev. Mod. Phys.* **83**, 1057 (2011).
- [2] M. Z. Hasan and C. L. Kane, Colloquium: Topological Insulators, *Rev. Mod. Phys.* **82**, 3045 (2010).
- [3] N. P. Armitage, E. J. Mele, and A. Vishwanath, Weyl and Dirac semimetals in three-dimensional solids, *Rev. Mod. Phys.* **90**, 015001 (2018).
- [4] A. Kitaev, Periodic table for topological insulators and superconductors, *AIP Conf. Proc.* **1134**, 22 (2009).
- [5] L. Fu, Topological Crystalline Insulators, *Phys. Rev. Lett.* **106**, 106802 (2011).
- [6] R.-J. Slager, A. Mesaros, V. Juričić, and J. Zaanen, The space group classification of topological band-insulators, *Nat. Phys.* **9**, 98 (2012).
- [7] J. Kruthoff, J. de Boer, J. van Wezel, C. L. Kane, and R.-J. Slager, Topological Classification of Crystalline Insulators through Band Structure Combinatorics, *Phys. Rev. X* **7**, 041069 (2017).
- [8] H. C. Po, A. Vishwanath, and H. Watanabe, Symmetry-based indicators of band topology in the 230 space groups, *Nat. Commun.* **8**, 50 (2017).
- [9] R.-J. Slager, The translational side of topological band insulators, *J. Phys. Chem. Solids* **128**, 24 (2019), spin-Orbit Coupled Materials.
- [10] B. Bradlyn, L. Elcoro, J. Cano, M. G. Vergniory, Z. Wang, C. Felser, M. I. Aroyo, and B. A. Bernevig, Topological quantum chemistry, *Nature* **547**, 298 (2017).
- [11] A. Bouhon, T. Bzdusek, and R.-J. Slager, Geometric approach to fragile topology beyond symmetry indicators, *Phys. Rev. B* **102**, 115135 (2020).
- [12] A. Bouhon, Q. Wu, R.-J. Slager, H. Weng, O. V. Yazyev, and T. Bzdusek, Non-Abelian reciprocal braiding of Weyl points and its manifestation in ZrTe, *Nature Physics* **16**, 1137 (2020).
- [13] J. Ahn, S. Park, and B.-J. Yang, Failure of Nielsen-Ninomiya Theorem and Fragile Topology in Two-Dimensional Systems with Space-Time Inversion Symmetry: Application to Twisted Bilayer Graphene at Magic Angle, *Phys. Rev. X* **9**, 021013 (2019).
- [14] A. Bouhon and R.-J. Slager, Multi-gap topological conversion of Euler class via band-node braiding: minimal models, *PT*-linked nodal rings, and chiral heirs (2022), [arXiv:2203.16741 \[cond-mat.mes-hall\]](https://arxiv.org/abs/2203.16741).
- [15] A. Bouhon, A. M. Black-Schaffer, and R.-J. Slager, Wilson loop approach to fragile topology of split elementary band representations and topological crystalline insulators with time-reversal symmetry, *Phys. Rev. B* **100**, 195135 (2019).
- [16] Q. Wu, A. A. Soluyanov, and T. Bzdusek, Non-Abelian band topology in noninteracting metals, *Science* **365**, 1273 (2019).
- [17] G. E. Volovik and V. P. Mineev, Investigation of singularities in superfluid He³ in liquid crystals by the homotopic topology methods, in *Basic Notions Of Condensed Matter Physics* (CRC Press, 2018) pp. 392–401.
- [18] A. J. Beekman, J. Nissinen, K. Wu, K. Liu, R.-J. Slager, Z. Nussinov, V. Cvetkovic, and J. Zaanen, Dual gauge field theory of quantum liquid crystals in two dimensions, *Phys. Rep.* **683**, 1 (2017), dual gauge field theory of quantum liquid crystals in two dimensions.
- [19] K. Liu, J. Nissinen, R.-J. Slager, K. Wu, and J. Zaanen, Generalized liquid crystals: Giant fluctuations and the vestigial chiral order of *i*, *o*, and *t* matter, *Phys. Rev. X* **6**, 041025 (2016).
- [20] G. P. Alexander, B. G.-g. Chen, E. A. Matsumoto, and R. D. Kamien, Colloquium: Disclination loops, point de-

- fects, and all that in nematic liquid crystals, *Rev. Mod. Phys.* **84**, 497 (2012).
- [21] W. J. Jankowski, M. Noormandipour, A. Bouhon, and R.-J. Slager, Disorder-induced topological quantum phase transitions in Euler semimetals (2023), [arXiv:2306.13084](https://arxiv.org/abs/2306.13084) [cond-mat.mes-hall].
- [22] J. Ahn and B.-J. Yang, Symmetry representation approach to topological invariants in $C_{2z}T$ -symmetric systems, *Phys. Rev. B* **99**, 235125 (2019).
- [23] W. J. Jankowski, A. S. Morris, A. Bouhon, F. N. Ünal, and R.-J. Slager, Optical manifestations of topological Euler class in electronic materials (2023), [arXiv:2311.07545](https://arxiv.org/abs/2311.07545) [cond-mat.mes-hall].
- [24] R.-J. Slager, A. Bouhon, and F. N. Ünal, Non-Abelian Floquet braiding and anomalous Dirac string phase in periodically driven systems, *Nature Communications* **15**, 1144 (2024).
- [25] F. N. Ünal, A. Bouhon, and R.-J. Slager, Topological Euler class as a dynamical observable in optical lattices, *Phys. Rev. Lett.* **125**, 053601 (2020).
- [26] W. Zhao, Y.-B. Yang, Y. Jiang, Z. Mao, W. Guo, L. Qiu, G. Wang, L. Yao, L. He, Z. Zhou, Y. Xu, and L. Duan, Quantum simulation for topological Euler insulators, *Communications Physics* **5**, 223 (2022).
- [27] B. Peng, A. Bouhon, B. Monserrat, and R.-J. Slager, Phonons as a platform for non-Abelian braiding and its manifestation in layered silicates, *Nature Communications* **13**, 423 (2022).
- [28] B. Peng, A. Bouhon, R.-J. Slager, and B. Monserrat, Multigap topology and non-Abelian braiding of phonons from first principles, *Phys. Rev. B* **105**, 085115 (2022).
- [29] A. Bouhon, G. F. Lange, and R.-J. Slager, Topological correspondence between magnetic space group representations and subdimensions, *Phys. Rev. B* **103**, 245127 (2021).
- [30] S. Chen, A. Bouhon, R.-J. Slager, and B. Monserrat, Non-Abelian braiding of Weyl nodes via symmetry-constrained phase transitions, *Phys. Rev. B* **105**, L081117 (2022).
- [31] Q. Guo, T. Jiang, R.-Y. Zhang, L. Zhang, Z.-Q. Zhang, B. Yang, S. Zhang, and C. T. Chan, Experimental observation of non-Abelian topological charges and edge states, *Nature* **594**, 195 (2021).
- [32] B. Jiang, A. Bouhon, S.-Q. Wu, Z.-L. Kong, Z.-K. Lin, R.-J. Slager, and J.-H. Jiang, Experimental observation of meronic topological acoustic Euler insulators (2022), [arXiv:2205.03429](https://arxiv.org/abs/2205.03429) [cond-mat.mes-hall].
- [33] B. Jiang, A. Bouhon, Z.-K. Lin, X. Zhou, B. Hou, F. Li, R.-J. Slager, and J.-H. Jiang, Experimental observation of non-Abelian topological acoustic semimetals and their phase transitions, *Nature Physics* **17**, 1239 (2021).
- [34] H. Qiu, Q. Zhang, T. Liu, X. Fan, F. Zhang, and C. Qiu, Minimal non-Abelian nodal braiding in ideal metamaterials (2022), [arXiv:2202.01467](https://arxiv.org/abs/2202.01467) [cond-mat.other].
- [35] Y. Yang, B. Yang, G. Ma, J. Li, S. Zhang, and C. T. Chan, Non-Abelian physics in light and sound (2023), [arXiv:2305.12206](https://arxiv.org/abs/2305.12206) [physics.optics].
- [36] F. D. M. Haldane, Model for a quantum Hall effect without Landau levels: Condensed-matter realization of the "parity anomaly", *Phys. Rev. Lett.* **61**, 2015 (1988).
- [37] T. Morimoto, Y. Hatsugai, and H. Aoki, Optical Hall conductivity in ordinary and graphene quantum Hall systems, *Phys. Rev. Lett.* **103**, 116803 (2009).
- [38] D. T. Tran, A. Dauphin, A. G. Grushin, P. Zoller, and N. Goldman, Probing topology by "heating": Quantized circular dichroism in ultracold atoms, *Science Advances* **3**, e1701207 (2017), <https://www.science.org/doi/pdf/10.1126/sciadv.1701207>.
- [39] L. Asteria, D. T. Tran, T. Ozawa, M. Tarnowski, B. S. Rem, N. Fläschner, K. Sengstock, N. Goldman, and C. Weitenberg, Measuring quantized circular dichroism in ultracold topological matter, *Nature Physics* **15**, 449 (2019).
- [40] F. de Juan, A. G. Grushin, T. Morimoto, and J. E. Moore, Quantized circular photogalvanic effect in Weyl semimetals, *Nature Communications* **8**, 10.1038/ncomms15995 (2017).
- [41] D. E. Parker, T. Morimoto, J. Orenstein, and J. E. Moore, Diagrammatic approach to nonlinear optical response with application to Weyl semimetals, *Physical Review B* **99**, 10.1103/physrevb.99.045121 (2019).
- [42] A. Avdoshkin, V. Kozii, and J. E. Moore, Interactions remove the quantization of the chiral photocurrent at Weyl points, *Physical Review Letters* **124**, 10.1103/physrevlett.124.196603 (2020).
- [43] J. Orenstein, J. Moore, T. Morimoto, D. Torchinsky, J. Harter, and D. Hsieh, Topology and symmetry of quantum materials via nonlinear optical responses, *Annual Review of Condensed Matter Physics* **12**, 247 (2021), <https://doi.org/10.1146/annurev-conmatphys-031218-013712>.
- [44] J. Provost and G. Vallee, Riemannian structure on manifolds of quantum states, *Communications in Mathematical Physics* **76**, 289 (1980).
- [45] R. Resta, The insulating state of matter: a geometrical theory, *The European Physical Journal B* **79**, 121 (2011).
- [46] S. Peotta and P. Törmä, Superfluidity in topologically nontrivial flat bands, *Nature communications* **6**, 1 (2015).
- [47] F. Xie, Z. Song, B. Lian, and B. A. Bernevig, Topology-bounded superfluid weight in twisted bilayer graphene, *Phys. Rev. Lett.* **124**, 167002 (2020).
- [48] N. Verma, T. Hazra, and M. Randeria, Optical spectral weight, phase stiffness, and Tc bounds for trivial and topological flat band superconductors, *Proceedings of the National Academy of Sciences* **118**, e2106744118 (2021), <https://www.pnas.org/doi/pdf/10.1073/pnas.2106744118>.
- [49] J. Mitscherling and T. Holder, Bound on resistivity in flat-band materials due to the quantum metric, *Phys. Rev. B* **105**, 085154 (2022).
- [50] P. Törmä, Essay: Where can quantum geometry lead us?, *Phys. Rev. Lett.* **131**, 240001 (2023).
- [51] J. Ahn, G.-Y. Guo, N. Nagaosa, and A. Vishwanath, Riemannian geometry of resonant optical responses, *Nature Physics* **18**, 290 (2021).
- [52] A. Bouhon, A. Timmel, and R.-J. Slager, Quantum geometry beyond projective single bands, *arXiv preprint arXiv:2303.02180* (2023).
- [53] H. Lim, S. Kim, and B.-J. Yang, Real Hopf insulator, *Phys. Rev. B* **108**, 125101 (2023).
- [54] Z. Davoyan, W. J. Jankowski, A. Bouhon, and R.-J. Slager, \mathcal{PT} -symmetric topological phases with Pontryagin index in three spatial dimensions (2023), [arXiv:2308.15555](https://arxiv.org/abs/2308.15555) [cond-mat.mes-hall].
- [55] T. Morimoto and N. Nagaosa, Topological nature of nonlinear optical effects in solids, *Science Advances* **2**, e1501524 (2016), <https://www.science.org/doi/pdf/10.1126/sciadv.1501524>.

- [56] J. E. Sipe and E. Ghahramani, Nonlinear optical response of semiconductors in the independent-particle approximation, *Phys. Rev. B* **48**, 11705 (1993).
- [57] J. E. Sipe and A. I. Shkrebtii, Second-order optical response in semiconductors, *Phys. Rev. B* **61**, 5337 (2000).
- [58] A. Alexandradinata, A topological principle for photovoltaics: Shift current in intrinsically polar insulators (2022), [arXiv:2203.11225 \[cond-mat.mes-hall\]](https://arxiv.org/abs/2203.11225).
- [59] Q. Ma, S.-Y. Xu, C.-K. Chan, C.-L. Zhang, G. Chang, Y. Lin, W. Xie, T. Palacios, H. Lin, S. Jia, P. A. Lee, P. Jarillo-Herrero, and N. Gedik, Direct optical detection of Weyl fermion chirality in a topological semimetal, *Nature Physics* **13**, 842–847 (2017).
- [60] H.-C. Hsu, J.-S. You, J. Ahn, and G.-Y. Guo, Nonlinear photoconductivities and quantum geometry of chiral multifold fermions, *Phys. Rev. B* **107**, 155434 (2023).
- [61] J. Ahn, Topological enhancement of nonlinear transport in unconventional point-node semimetals, *Phys. Rev. B* **107**, L201112 (2023).
- [62] J. Ahn and B. Ghosh, Topological circular dichroism in chiral multifold semimetals, *Phys. Rev. Lett.* **131**, 116603 (2023).
- [63] H. Watanabe and Y. Yanase, Chiral photocurrent in parity-violating magnet and enhanced response in topological antiferromagnet, *Phys. Rev. X* **11**, 011001 (2021).
- [64] H. Watanabe and Y. Yanase, Photocurrent response in parity-time symmetric current-ordered states, *Phys. Rev. B* **104**, 024416 (2021).
- [65] M. M. Otrokov, I. I. Klimovskikh, H. Bentmann, D. Estyunin, A. Zeugner, Z. S. Aliev, S. Gaß, A. U. B. Wolter, A. V. Koroleva, A. M. Shikin, M. Blanco-Rey, M. Hoffmann, I. P. Rusinov, A. Y. Vyazovskaya, S. V. Ere-meev, Y. M. Koroteev, V. M. Kuznetsov, F. Freyre, J. Sánchez-Barriga, I. R. Amiraslanov, M. B. Babanly, N. T. Mamedov, N. A. Abdullayev, V. N. Zverev, A. Alfonso, V. Kataev, B. Büchner, E. F. Schwier, S. Kumar, A. Kimura, L. Petaccia, G. Di Santo, R. C. Vidal, S. Schatz, K. Kißner, M. Ünzelmann, C. H. Min, S. Moser, T. R. F. Peixoto, F. Reinert, A. Ernst, P. M. Echenique, A. Isaeva, and E. V. Chulkov, Prediction and observation of an antiferromagnetic topological insulator, *Nature* **576**, 416 (2019).
- [66] R. S. K. Mong, A. M. Essin, and J. E. Moore, Antiferromagnetic topological insulators, *Phys. Rev. B* **81**, 245209 (2010).
- [67] N. H. Jo, L.-L. Wang, R.-J. Slager, J. Yan, Y. Wu, K. Lee, B. Schunk, A. Vishwanath, and A. Kaminski, Intrinsic axion insulating behavior in antiferromagnetic MnBi₆Te₁₀, *Phys. Rev. B* **102**, 045130 (2020).
- [68] A. Gao, Y.-F. Liu, J.-X. Qiu, B. Ghosh, T. V. Trevisan, Y. Onishi, C. Hu, T. Qian, H.-J. Tien, S.-W. Chen, M. Huang, D. Bérubé, H. Li, C. Tzschaschel, T. Dinh, Z. Sun, S.-C. Ho, S.-W. Lien, B. Singh, K. Watanabe, T. Taniguchi, D. C. Bell, H. Lin, T.-R. Chang, C. R. Du, A. Bansil, L. Fu, N. Ni, P. P. Orth, Q. Ma, and S.-Y. Xu, Quantum metric nonlinear Hall effect in a topological antiferromagnetic heterostructure, *Science* **381**, 181–186 (2023).
- [69] S. Chen, S. Chaudhary, G. Refael, and C. Lewandowski, Enhancing shift current via virtual multiband transitions (2024), [arXiv:2402.06721 \[cond-mat.mes-hall\]](https://arxiv.org/abs/2402.06721).
- [70] A. Zee, *Quantum Field Theory in a Nutshell* (Princeton University Press, 2010).

Appendix A: Basic quantum-geometric definitions

In this section, for completeness, we define the relevant quantum-geometric objects within the single-particle picture of Bloch states, as originally introduced in Ref. [44] and extended towards optical responses in Ref. [51]. We start with the quantum-geometric tensor (QGT) for bands m, n mentioned in the main text,

$$Q_{ab}^{mn} \equiv r_{nm}^a r_{mn}^b. \quad (\text{A1})$$

Here, the transition dipole moment vector, $\mathbf{r}_{mn}(\mathbf{k}) = \langle \psi_{m,\mathbf{k}} | \hat{\mathbf{r}} | \psi_{n,\mathbf{k}} \rangle$, provides a probability amplitude for an electric dipole (E1) transition between Bloch states $|\psi_{n,\mathbf{k}}\rangle$ and $|\psi_{m,\mathbf{k}}\rangle$. More abstractly, \mathbf{r}_{mn} defines a tangent vector on the manifold of quantum states [51], with components

$$\mathbf{r}_{mn}^a(\mathbf{k}) = i(1 - \delta_{mn})A_{nm}^a(\mathbf{k}), \quad (\text{A2})$$

where $A_{nm}^a(\mathbf{k}) \equiv \langle u_{n,\mathbf{k}} | \partial_a u_{m,\mathbf{k}} \rangle$ is the non-Abelian Berry connection, and we employ a simplified notation $\partial_a \equiv \partial_{k_a}$.

The QGT, known otherwise as Hermitian metric, decomposes as

$$Q_{ab}^{mn} = g_{ab}^{mn} - \frac{i}{2} F_{ab}^{mn}, \quad (\text{A3})$$

and equips the vector bundle of Bloch states [52] over a Brillouin zone (BZ), $\text{BZ} \cong T^d$, where T^d is a d -dimensional torus, with a Riemannian structure through its real part $g_{ab}^{mn} = \Re Q_{ab}^{mn}$, the quantum metric. In particular g_{ab}^{mn} defines a Fubini-Study metric through $g_n^{ab} = \sum_m^{\text{unocc}} g_{ab}^{mn}$,

$$ds_n^2 \equiv 1 - |\langle u_{n,\mathbf{k}} | u_{n,\mathbf{k}+\delta\mathbf{k}} \rangle|^2 = g_n^{ab} dk_a dk_b, \quad (\text{A4})$$

for any band n . The symplectic part F_{ab}^{mn} yields the Abelian Berry curvature $F_{ab}^n = \sum_m^{\text{unocc}} F_{ab}^{mn}$ on performing a summation over the unoccupied bands.

Furthermore, for higher order in k -space derivatives, the Hermitian connection can be defined. The advantage of the described representation is that it allows to easily introduce a Hermitian connection as

$$C_{bca}^{mn} \equiv r_{nm}^b r_{mn}^{c;a}, \quad (\text{A5})$$

where we include the covariant derivative $r_{nm}^{b;c}$ of the transition dipole, defined in terms of the Berry connection as

$$r_{nm}^{c;a}(\mathbf{k}) = \nabla_a r_{nm}^c(\mathbf{k}) = \partial_a r_{nm}^c(\mathbf{k}) - i(A_{nn}^a(\mathbf{k}) - A_{mm}^a(\mathbf{k}))r_{nm}^c(\mathbf{k}). \quad (\text{A6})$$

The formal definition in terms of covariant derivative can be directly recast into the shift vector definition introduced in the main text.

Furthermore, the Hermitian connection can be decomposed in terms of the metric connection $\Re C_{abc}^{mn}$ and symplectic connection $\Im C_{abc}^{mn}$ as

$$C_{abc}^{mn} = \Re C_{abc}^{mn} + i\Im C_{abc}^{mn}. \quad (\text{A7})$$

The *torsion-free* part of the metric connection $\Re C_{abc}^{mn}$ reads [22],

$$\Gamma_{abc}^{mn} = \frac{1}{2}(\partial_b g_{ac}^{mn} + \partial_c g_{ab}^{mn} - \partial_a g_{bc}^{mn}), \quad (\text{A8})$$

but this part crucially omits the virtual transitions, essential for the optical responses of the non-Abelian topological insulators. The torsion tensor $T_{abc}^{mn} \equiv C_{abc}^{mn} - C_{acb}^{mn}$, as defined in the main text, explicitly captures the virtual transitions as [51],

$$T_{abc}^{mn} = i \sum_{i,j} r_{n_i m_j}^a \sum_{E_p \neq E_m, E_n} (r_{m_j p}^b r_{pn_i}^c - r_{m_j p}^c r_{pn_i}^b), \quad (\text{A9})$$

on direct substitution in terms of r_{mn}^a transition dipole matrix elements. Here, we account for the degeneracies, by labelling energies of the (degenerate) electronic eigenstates at given momentum \mathbf{k} , as $E_n = E_{n_i}$. Here, explicitly, the torsion tensor elements combine the E1 transition amplitudes given by the transition dipole matrix elements r_{nm}^a for (i) starting from a occupied band n , (ii) virtually exciting an electron through band p , and (iii) finally ending up photoexcited in initially unoccupied band m .

We note that in particular, if the Bloch states can be chosen in the real gauge, i.e. $|u_{n,\mathbf{k}}\rangle$ become real vectors, under the so-called reality condition (see Appendix B), $C_{abc} = \Re C_{abc}$, as follows from a direct substitution of Bloch states to the transition dipole moment matrix elements.

Appendix B: Non-Abelian three-dimensional topologies under the reality condition

In this section, we first clarify the constraints due to the reality condition imposed by the \mathcal{PT} symmetry imposed on three-dimensional non-Abelian topological phases. Regarding the latter, we provide simple models and elaborate on the topologies of (i) multi-gap flag phases, (ii) the real Hopf insulator, (iii) Pontryagin-indexed insulator, all of which can be generated and characterized within the Plücker formalism framework [11, 52].

1. Reality condition

The action of the \mathcal{PT} symmetry (here, we consider spinless $(\mathcal{PT})^2 = +1$ symmetry) ensures that the Bloch Hamiltonian of a three-dimensional solid treated within an independent-particle approximation is real, $H(\mathbf{k}) = H^*(\mathbf{k})$, and there exists a gauge in which the associated eigenstates labelled with quasimomenta $\mathbf{k} = (k_x, k_y, k_z)^T$ are also real vectors. In particular, this follows from the symmetry transformations of the Hamiltonian [11]:

$$(\mathcal{PT})H(k_x, k_y, k_z)(\mathcal{PT})^{-1} = H^*(k_x, k_y, k_z) = H(k_x, k_y, k_z), \quad (\text{B1})$$

which is related to the fact that the individual symmetries of the composed symmetry act as:

$$\mathcal{T}H(k_x, k_y, k_z)\mathcal{T}^{-1} = H^*(-k_x, -k_y, -k_z), \quad (\text{B2})$$

$$\mathcal{P}H(k_x, k_y, k_z)\mathcal{P}^{-1} = H(-k_x, -k_y, -k_z). \quad (\text{B3})$$

Hence, the Bloch Hamiltonian, $H(k_x, k_y, k_z) = H^*(k_x, k_y, k_z)$, can be represented as a real matrix [11]. Combined with the Hermiticity of the Hamiltonian, the Hamiltonian indeed reduces to a real *symmetric* matrix, therefore it enjoys a well-known property that its eigenvectors can be taken real, $|u_{n,\mathbf{k}}\rangle \in \mathbb{R}^N$.

Therefore, we note that under such reality condition imposed by the \mathcal{PT} symmetry,

$$\mathbf{A}_{nn}(\mathbf{k}) = i\langle u_{n,\mathbf{k}}|\nabla_{\mathbf{k}}u_{n,\mathbf{k}}\rangle = i\nabla_{\mathbf{k}}\langle u_{n,\mathbf{k}}|u_{n,\mathbf{k}}\rangle - i\langle \nabla_{\mathbf{k}}u_{n,\mathbf{k}}|u_{n,\mathbf{k}}\rangle = -i\langle u_{n,\mathbf{k}}|\nabla_{\mathbf{k}}u_{n,\mathbf{k}}\rangle = -\mathbf{A}_{nn}(\mathbf{k}), \quad (\text{B4})$$

using (i) a product rule, (ii) normalization condition imposed on the eigenvectors, and (iii) complex conjugation of a real inner product. Hence, $\mathbf{A}_{nn}(\mathbf{k}) = 0$, i.e. the diagonal elements of the non-Abelian Berry connection, as well as its trace, vanish identically; as a result of imposing the reality condition on the Hamiltonian.

2. Multi-gap flag phases

Here, we provide details on non-Abelian real topology of multi-gap flag phases, including the construction of relevant models encoded in corresponding Bloch Hamiltonians. As introduced in Ref. [54], the multi-gap flag phases with four isolated bands are classified by the homotopy of flag varieties, $\tilde{\text{Fl}}_{p_1, \dots, p_k}(\mathbb{R}) \equiv SO(\sum_{i=1}^k p_i)/[SO(p_1) \times \dots \times SO(p_k)]$, where $p_1, \dots, p_k \in \mathbb{N}$ are numbers of bands in the gapped subbundles. Here, $p_1 = p_2 = p_3 = p_4 = 1$, with:

$$\tilde{\text{Fl}}_{1,1,1,1}(\mathbb{R}) = SO(4) \cong \frac{S^3 \times S^3}{\mathbb{Z}_2}. \quad (\text{B5})$$

Namely, we have $\pi_3(\text{Fl}_{1,1,1,1}(\mathbb{R})) \cong \pi_3(SO(4)) \cong \mathbb{Z} \oplus \mathbb{Z} = \mathbb{Z}^2$.

To interpret the meaning of the \mathbb{Z}^2 invariant, we recall the well-known isomorphism,

$$SO(4) \cong \frac{S_L^3 \times S_R^3}{\mathbb{Z}_2}, \quad (\text{B6})$$

which on recognizing that the \mathbb{Z}_2 quotient does not affect π_n for $n \geq 2$, allows to interpret the invariant as a pair of windings on two copies of 3-spheres,

$$\pi_3(S_L^3 \times S_R^3) \cong \pi_3(S_L^3) \oplus \pi_3(S_R^3) \cong \mathbb{Z} \oplus \mathbb{Z}. \quad (\text{B7})$$

We recognize that the non-trivial $S^3 \rightarrow S^3$ maps corresponding to the non-trivial elements of $\pi_3(S_{L/R}^3) \cong \mathbb{Z}$ can be interpreted as winding numbers w_L, w_R .

Correspondingly, we construct the flag Hamiltonian by taking:

$$H(\mathbf{k}) = V(\mathbf{k}) \text{diag}[E_1, E_2, E_3, E_4] V(\mathbf{k})^T, \quad (\text{B8})$$

with $E_1 < E_2 < E_3 < E_4$ introducing three gaps, and $V = V_R V_L^T$ which can be factored in terms of two matrices introducing the isoclinic windings. These can be constructed as

$$V_L = \begin{pmatrix} l_0 & -l_3 & l_2 & -l_1 \\ l_3 & l_0 & -l_1 & -l_2 \\ -l_2 & l_1 & l_0 & -l_3 \\ l_1 & l_2 & l_3 & l_0 \end{pmatrix}, \quad (\text{B9})$$

$$V_R = \begin{pmatrix} r_0 & -r_3 & r_2 & r_1 \\ r_3 & r_0 & -r_1 & r_2 \\ -r_2 & r_1 & r_0 & r_3 \\ -r_1 & -r_2 & -r_3 & r_0 \end{pmatrix}, \quad (\text{B10})$$

with $l_0^2 + l_1^2 + l_2^2 + l_3^2 = 1$ and $r_0^2 + r_1^2 + r_2^2 + r_3^2 = 1$. On such factorization, the invariants of the flag phases can be directly deduced from the following formulae of the winding invariants:

$$\begin{aligned} w_L &= \frac{1}{2\pi^2} \int_{\text{BZ}} d^3\mathbf{k} \epsilon_{ijpq} l^i \partial_{k_x} l^j \partial_{k_y} l^p \partial_{k_z} l^q, \\ w_R &= \frac{1}{2\pi^2} \int_{\text{BZ}} d^3\mathbf{k} \epsilon_{ijpq} r^i \partial_{k_x} r^j \partial_{k_y} r^p \partial_{k_z} r^q. \end{aligned} \quad (\text{B11})$$

In particular, we can model these by a choice

$$(l_0, l_1, l_2, l_3) = (\sin w_L k_x, \sin k_y, \sin k_z, M - \cos w_L k_x - \cos k_y - \cos k_z)^T, \quad (\text{B12})$$

$$(r_0, r_1, r_2, r_3) = (\sin w_R k_x, \sin k_y, \sin k_z, M - \cos w_R k_x - \cos k_y - \cos k_z)^T. \quad (\text{B13})$$

where we set the topological mass to $M = 2$. Additionally, changing the parameter M allows to induce topological phase transitions (TPTs), on gap closings, as shown explicitly in the main text.

3. Real Hopf insulator

In the case of a real Hopf insulator we consider the $2 \oplus 2$ band partitioning. In terms of homotopy classification of the topological phases encoded with real topologies [11], the band partitioning yields a classification on an oriented real Grassmannian manifold,

$$\widetilde{\text{Gr}}_{2,4}(\mathbb{R}) = SO(4)/(SO(2) \times SO(2)) \cong S^2 \times S^2. \quad (\text{B14})$$

Therefore, the invariant can be obtained as $\pi_3(\widetilde{\text{Gr}}_{2,4}) \cong \pi_3(S^2 \times S^2) \cong \pi_3(S^2) \oplus \pi_3(S^2) \cong \mathbb{Z} \oplus \mathbb{Z}$, where each $\pi_3(S^2) \cong \mathbb{Z}$ defines a Hopf fibration ($S^3 \rightarrow S^2$) and an associated Hopf index.

Following Ref. [53], these Hopf invariants can be written as:

$$\begin{aligned} \chi_z &= -\frac{1}{16\pi^2} \int_{BZ} \mathbf{a}^c \wedge \text{Eu}^c + \mathbf{a}^v \wedge \text{Eu}^v + \mathbf{a}^c \wedge \text{Eu}^v + \mathbf{a}^v \wedge \text{Eu}^c \in \mathbb{Z}, \\ \chi_w &= -\frac{1}{16\pi^2} \int_{BZ} \mathbf{a}^c \wedge \text{Eu}^c + \mathbf{a}^v \wedge \text{Eu}^v - \mathbf{a}^c \wedge \text{Eu}^v - \mathbf{a}^v \wedge \text{Eu}^c \in \mathbb{Z}. \end{aligned} \quad (\text{B15})$$

In particular, we notice that on summation, the invariants yield

$$\chi_z + \chi_w = -\frac{1}{8\pi^2} \int_{BZ} \mathbf{a}^c \wedge \text{Eu}^c + \mathbf{a}^v \wedge \text{Eu}^v \in \mathbb{Z} \quad (\text{B16})$$

which is the quantized number entering the integrated shift response introduced in the main text.

The models for real Hopf insulators can be obtained from a flattened Hamiltonian ensuring a correct band partitioning

$$H^{\chi_z, \chi_w}(\mathbf{k}) = R_{z,w}(\mathbf{k}) \text{diag}[-1, -1, 1, 1] R_{z,w}^T(\mathbf{k}), \quad (\text{B17})$$

where $R_{z,w}(\mathbf{k})$ encodes the double Hopf fibration inducing indices (χ_w, χ_z) , as introduced and discussed in detail in Ref. [53].

4. Pontryagin-indexed insulator

To define the insulator with Pontryagin index, we demand a $3 \oplus 1$ partitioning of four topological bands. From the homotopy perspective, the effective classifying space of interest becomes a oriented real Grassmannian,

$$\widetilde{\text{Gr}}_{1,4}(\mathbb{R}) = SO(4)/SO(3) \cong S^3, \quad (\text{B18})$$

as discussed in Ref. [54]. The homotopy classification in three spatial dimensions then gives

$$\pi_3(\widetilde{\text{Gr}}_{1,4}(\mathbb{R})) \cong \pi_3(S^3) \cong \mathbb{Z}, \quad (\text{B19})$$

where indeed $\pi_3(S^3) \cong \mathbb{Z}$ defines the Pontryagin index Q , which classifies homotopy-inequivalent maps: $S^3 \rightarrow S^3$ [70].

The Pontryagin index can be computed from the non-Abelian Berry connection elements as

$$Q = \frac{1}{2\pi^2} \int_{T^3} d^3k \epsilon^{ijk} A_{41}^i A_{42}^j A_{43}^k. \quad (\text{B20})$$

Equivalently [54], the invariant can be computed as the winding of the fourth band $\mathbf{u}_4 \equiv |u_{4,\mathbf{k}}\rangle$ as,

$$Q = \frac{1}{2\pi^2} \int_{S^3} d^3k \epsilon_{ijpq} (\mathbf{u}_4)^i \partial_{k_x} (\mathbf{u}_4)^j \partial_{k_y} (\mathbf{u}_4)^p \partial_{k_z} (\mathbf{u}_4)^q, \quad (\text{B21})$$

pushed forward to a 3-sphere S^3 from the BZ 3-torus ($T^3 \rightarrow S^3$). As shown in Ref. [54], to generate a concrete model, one could take a flattened Hamiltonian and a Bloch band matrix $R(\mathbf{k})$ as

$$H^Q(\mathbf{k}) = R(\mathbf{k}) \begin{pmatrix} -1 & 0 & 0 & 0 \\ 0 & 1 & 0 & 0 \\ 0 & 0 & 1 & 0 \\ 0 & 0 & 0 & 1 \end{pmatrix} R(\mathbf{k})^T. \quad (\text{B22})$$

Here, the matrix $R(\mathbf{k}) \in SO(4)$ can be obtained by a three-angle parametrization (ϕ, ψ, θ) obtained from Plücker formalism, namely [11, 54]:

$$\psi(\mathbf{k}) = \pi \max\{|k_x|, |k_y|, |k_z|\}, \quad (\text{B23})$$

$$\theta(\mathbf{k}) = \cos^{-1}(k_z / \sqrt{k_x^2 + k_y^2 + k_z^2}), \quad (\text{B24})$$

$$\phi(\mathbf{k}) = Q \tan^{-1}(k_x/k_y), \quad (\text{B25})$$

deduced for any k -point in the BZ. Correspondingly, the Bloch matrix inducing $Q \neq 0$ can be generated as

$$R(\mathbf{k}) = e^{i\theta\Gamma_{20}} e^{i\phi\Gamma_{21}} e^{i\psi\Gamma_{12}}. \quad (\text{B26})$$

Having revised the possible non-Abelian four-band topology in three spatial dimensions we note however that the optical shift responses induced by the Pontryagin index on occupying the entire three-band subspace do not yield a 3-form resulting in a quantized response, contrary to the topology of real Hopf insulators and the multi-gap flag phases discussed above. On the other hand, the Pontryagin-indexed insulators can be doped, such that only two bands are occupied, as the Fermi level is set at band crossings, and in that case the quantized shift response can be realized on photoexcitations. For the derivation of the quantized responses, see Appendix D.

Appendix C: Torsional representation of symmetrized circular shift photoconductivities

As introduced in the main text, the circular shift photoconductivity $\sigma_{\text{shift,C}}^{cab}(\omega)$ in terms of the metric connection $C_{bca}^{mn} = (C_{bca}^{mn})^* = \Re C_{bca}^{mn}$, under the reality condition (see also Appendix A), reads

$$\sigma_{\text{shift,C}}^{cab}(\omega) = -\frac{e^2}{8\pi^2\hbar^2} \int d^3k \sum_{m,n} f_{mn} \Re (C_{bca}^{mn} - C_{acb}^{mn}) \delta(\omega_{mn} - \omega). \quad (\text{C1})$$

Now, to derive the torsional representation of circular shift photoconductivities, we start by recognizing that the sum of circular shift photoconductivities can be written as:

$$\begin{aligned}
& \int d\omega (\sigma_{\text{shift,C}}^{abc}(\omega) + \sigma_{\text{shift,C}}^{bca}(\omega) + \sigma_{\text{shift,C}}^{cab}(\omega)) = \\
& = -\frac{e^2}{8\pi^2\hbar^2} \int d^3k \sum_{m,n} f_{mn} \left((\Re C_{cab}^{mn} - \Re C_{bac}^{mn}) + (\Re C_{abc}^{mn} - \Re C_{cba}^{mn}) + (\Re C_{bca}^{mn} - \Re C_{acb}^{mn}) \right) = \\
& = \frac{e^2}{8\pi^2\hbar^2} \int d^3k \sum_{m,n} f_{mn} \left((\Re C_{acb}^{mn} - \Re C_{abc}^{mn}) + (\Re C_{cba}^{mn} - \Re C_{cab}^{mn}) + (\Re C_{bac}^{mn} - \Re C_{bca}^{mn}) \right) = \\
& = \frac{e^3}{8\pi^2\hbar^2} \int d^3k \sum_{m,n} f_{mn} \Re (T_{acb}^{mn} + T_{cba}^{mn} + T_{bac}^{mn}),
\end{aligned} \tag{C2}$$

where the first equality follows directly from the Eq. (C1) of the main text on performing the integration over the frequencies, and second equality corresponds identically to reordering the terms. The third equality follows from the definition of the torsion tensor and decomposition of Hermitian connection into real (metric) and imaginary (symplectic) parts. Therefore, the sum of circular shift photoconductivities can be captured purely in terms of the torsion tensor.

Appendix D: Torsion tensor in non-Abelian topological phases satisfying the reality condition

First, we rewrite the torsion tensor in terms of the non-Abelian Berry connection, assuming that a symmetry imposing the reality condition is present,

$$T_{abc}^{mn} = A_{nm}^a \sum_{m \neq p \neq n} (A_{mp}^c A_{pn}^b - A_{mp}^b A_{pn}^c). \tag{D1}$$

Correspondingly, we have:

$$\begin{aligned}
T_{abc}^{mn} + T_{bca}^{mn} + T_{cab}^{mn} = & \sum_{m \neq p \neq n} (A_{nm}^a A_{mp}^c A_{pn}^b - A_{nm}^a A_{mp}^b A_{pn}^c + A_{nm}^b A_{mp}^a A_{pn}^c + \\
& - A_{nm}^b A_{mp}^c A_{pn}^a + A_{nm}^c A_{mp}^b A_{pn}^a - A_{nm}^c A_{mp}^a A_{pn}^b),
\end{aligned} \tag{D2}$$

which explicitly reflects the definitional nature of the torsion tensor capturing possible virtual transitions, here in terms of the non-Abelian Berry connection elements.

In the subsequent, we evaluate the symmetrized sum of the torsion tensor elements in the four-band and three-band setups of the non-Abelian topological insulators satisfying the reality condition, cf. Appendix B.

1. Torsion in four-band models

We start with the evaluation of the torsion tensor in the four-band models, relevant for the non-Abelian topologies studied in Refs. [53, 54].

Here, we assume that there are 2 occupied bands ($n = 1, 2$) and 2 unoccupied bands ($m = 3, 4$), obtaining:

$$\begin{aligned}
T_{abc}^{31} + T_{bca}^{31} + T_{cab}^{31} = & (A_{13}^a A_{32}^c A_{21}^b - A_{13}^a A_{32}^b A_{21}^c + A_{13}^b A_{32}^a A_{21}^c - A_{13}^b A_{32}^c A_{21}^a + A_{13}^c A_{32}^b A_{21}^a - A_{13}^c A_{32}^a A_{21}^b) + \\
& + (A_{13}^a A_{34}^c A_{41}^b - A_{13}^a A_{34}^b A_{41}^c + A_{13}^b A_{34}^a A_{41}^c - A_{13}^b A_{34}^c A_{41}^a + A_{13}^c A_{34}^b A_{41}^a - A_{13}^c A_{34}^a A_{41}^b),
\end{aligned} \tag{D3}$$

$$\begin{aligned}
T_{abc}^{41} + T_{bca}^{41} + T_{cab}^{41} = & (A_{14}^a A_{42}^c A_{21}^b - A_{14}^a A_{42}^b A_{21}^c + A_{14}^b A_{42}^a A_{21}^c - A_{14}^b A_{42}^c A_{21}^a + A_{14}^c A_{42}^b A_{21}^a - A_{14}^c A_{42}^a A_{21}^b) + \\
& + (A_{14}^a A_{43}^c A_{31}^b - A_{14}^a A_{43}^b A_{31}^c + A_{14}^b A_{43}^a A_{31}^c - A_{14}^b A_{43}^c A_{31}^a + A_{14}^c A_{43}^b A_{31}^a - A_{14}^c A_{43}^a A_{31}^b),
\end{aligned} \tag{D4}$$

$$\begin{aligned}
T_{abc}^{32} + T_{bca}^{32} + T_{cab}^{32} = & (A_{23}^a A_{31}^c A_{12}^b - A_{23}^a A_{31}^b A_{12}^c + A_{23}^b A_{31}^a A_{12}^c - A_{23}^b A_{31}^c A_{12}^a + A_{23}^c A_{31}^b A_{12}^a - A_{23}^c A_{31}^a A_{12}^b) + \\
& + (A_{23}^a A_{34}^c A_{42}^b - A_{23}^a A_{34}^b A_{42}^c + A_{23}^b A_{34}^a A_{42}^c - A_{23}^b A_{34}^c A_{42}^a + A_{23}^c A_{34}^b A_{42}^a - A_{23}^c A_{34}^a A_{42}^b),
\end{aligned} \tag{D5}$$

$$T_{abc}^{42} + T_{bca}^{42} + T_{cab}^{42} = (A_{24}^a A_{41}^c A_{12}^b - A_{24}^a A_{41}^b A_{12}^c + A_{24}^b A_{41}^a A_{12}^c - A_{24}^b A_{41}^c A_{12}^a + A_{24}^c A_{41}^b A_{12}^a - A_{24}^c A_{41}^a A_{12}^b) + (A_{24}^a A_{34}^c A_{32}^b - A_{24}^a A_{43}^b A_{32}^c + A_{24}^b A_{43}^a A_{32}^c - A_{24}^b A_{43}^c A_{32}^a + A_{24}^c A_{43}^b A_{32}^a - A_{24}^c A_{43}^a A_{32}^b). \quad (D6)$$

On summing all the terms and simplifying using $A_{ij}^a = -A_{ji}^a$ consistently with the reality condition (see Appendix B):

$$\begin{aligned} \sum_{m,n} (T_{abc}^{mn} + T_{bca}^{mn} + T_{cab}^{mn}) &= -2A_{12}^a (A_{13}^b A_{32}^c - A_{13}^c A_{32}^b + A_{14}^b A_{42}^c - A_{14}^c A_{42}^b) + \\ &-2A_{12}^b (A_{13}^c A_{32}^a - A_{13}^a A_{32}^c + A_{14}^c A_{42}^a - A_{14}^a A_{42}^c) - 2A_{12}^c (A_{13}^a A_{32}^b - A_{13}^b A_{32}^a + A_{14}^a A_{42}^b - A_{14}^b A_{42}^a) + \\ &-2A_{34}^a (A_{31}^b A_{14}^c - A_{31}^c A_{14}^b + A_{32}^b A_{24}^c - A_{32}^c A_{24}^b) + \\ &-2A_{34}^b (A_{31}^c A_{14}^a - A_{31}^a A_{14}^c + A_{32}^c A_{24}^a - A_{32}^a A_{24}^c) - 2A_{34}^c (A_{31}^a A_{14}^b - A_{31}^b A_{14}^a + A_{32}^a A_{24}^b - A_{32}^b A_{24}^a). \end{aligned} \quad (D7)$$

In terms of the two-band Euler connection: $\text{Eu}_{nm}^{ab} = \langle \partial_a u_n | \partial_b u_m \rangle - \langle \partial_b u_n | \partial_a u_m \rangle = \sum_{n \neq p \neq m} A_{np}^a A_{pm}^b - A_{np}^b A_{pm}^a$, where the second equality follows from resolution of identity $1 = \sum_p |u_p\rangle\langle u_p|$, and the reality condition ($A_{ii}^a = -A_{ii}^a = 0$). Hence:

$$\sum_{m,n} (T_{abc}^{mn} + T_{bca}^{mn} + T_{cab}^{mn}) = -2A_{12}^a \text{Eu}_{12}^{bc} - 2A_{12}^b \text{Eu}_{12}^{ca} - 2A_{12}^c \text{Eu}_{12}^{ab} - 2A_{34}^a \text{Eu}_{34}^{bc} - 2A_{34}^b \text{Eu}_{34}^{ca} - 2A_{34}^c \text{Eu}_{34}^{ab}. \quad (D8)$$

On identifying $\mathbf{a}^v = \mathbf{A}_{21} = -\mathbf{A}_{12}$, $\mathbf{a}^c = \mathbf{A}_{43} = -\mathbf{A}_{34}$, and finally $(\mathbf{Eu}^{v/c})_a = \epsilon_{abc} \text{Eu}_{1/3}^{bc}$, we retrieve:

$$\sum_{m,n} (T_{abc}^{mn} + T_{bca}^{mn} + T_{cab}^{mn}) = -2(\mathbf{a}^v \cdot \mathbf{Eu}^v + \mathbf{a}^c \cdot \mathbf{Eu}^c). \quad (D9)$$

In terms of the language of differential forms:

$$\sum_{m,n} (T_{abc}^{mn} + T_{bca}^{mn} + T_{cab}^{mn}) dk_x \wedge dk_y \wedge dk_z = -2(a^v \wedge \text{Eu}^v + a^c \wedge \text{Eu}^c), \quad (D10)$$

which is the 3-form integrated over the BZ $\cong T^3$ to find the sum of real Hopf invariants in the four-band case. Here, the Euler connections (1-forms) and curvatures (2-forms) are defined in terms of the pairs of conduction and valence bands $a^{v/c} = \langle u_{2/4} | d | u_{1/3} \rangle$, $\text{Eu}^{v/c} = da^{v/c}$. To demonstrate the non-triviality of the 3-form components, we plot the relevant torsion tensor components summed over bands $T_{xyz} \equiv \sum_{m,n} T_{xyz}^{mn}$, $T_{yzx} \equiv \sum_{m,n} T_{yzx}^{mn}$, $T_{zxy} \equiv \sum_{m,n} T_{zxy}^{mn}$ in the form of a vector field $(T_{xyz}, T_{yzx}, T_{zxy})$ over BZ torus, see Fig. 4. For the demonstration, we choose the real Hopf insulator model from the main text. We notice that significant contributions appear from the edge of BZ.

The BZ integral of the sum of the torsion tensor components yields quantized numbers reflected by the circular shift photoconductivity, as introduced in the main text. It should be stressed again that a four-band bundle, as modelled here in terms of the virtual transitions between four-bands (with amplitudes given by the elements of the non-Abelian Berry connection), can be selectively accessed by tuning the range of frequencies involved in non-linear optical transitions generating the circular shift current. Moreover, the four-band subspace needs to be isolated from the rest of the valence and conduction bands. Otherwise, the studied homotopy invariants can be trivialized [11], which emphasizes the multi-gap nature of these topological invariants. Finally, we notice that if the material is isotropic, then: $\sigma_{\text{shift}}^{xyz}(\omega) = \sigma_{\text{shift}}^{yzx}(\omega) = \sigma_{\text{shift}}^{zxy}(\omega)$. In that case, on combining with the final result of Appendix C, the shift photoconductivity integrates to a quantized value for *each* of the *individual* directions of light incidence, i.e. the necessity of combining all symmetrized directions to achieve the quantization condition is removed.

2. Torsion in three-band models

For completeness, we also introduce the derivation of the symmetrized sums of the torsion tensor elements for 3-band models under the reality condition (Appendix B). Now, we assume that there are 2 occupied bands ($n = 1, 2$) and 1 unoccupied band ($m = 3$), obtaining:

$$T_{abc}^{31} + T_{bca}^{31} + T_{cab}^{31} = (A_{13}^a A_{32}^c A_{21}^b - A_{13}^a A_{32}^b A_{21}^c + A_{13}^b A_{32}^a A_{21}^c - A_{13}^b A_{32}^c A_{21}^a + A_{13}^c A_{32}^b A_{21}^a - A_{13}^c A_{32}^a A_{21}^b), \quad (D11)$$

$$T_{abc}^{32} + T_{bca}^{32} + T_{cab}^{32} = (A_{23}^a A_{31}^c A_{12}^b - A_{23}^a A_{31}^b A_{12}^c + A_{23}^b A_{31}^a A_{12}^c - A_{23}^b A_{31}^c A_{12}^a + A_{23}^c A_{31}^b A_{12}^a - A_{23}^c A_{31}^a A_{12}^b). \quad (D12)$$

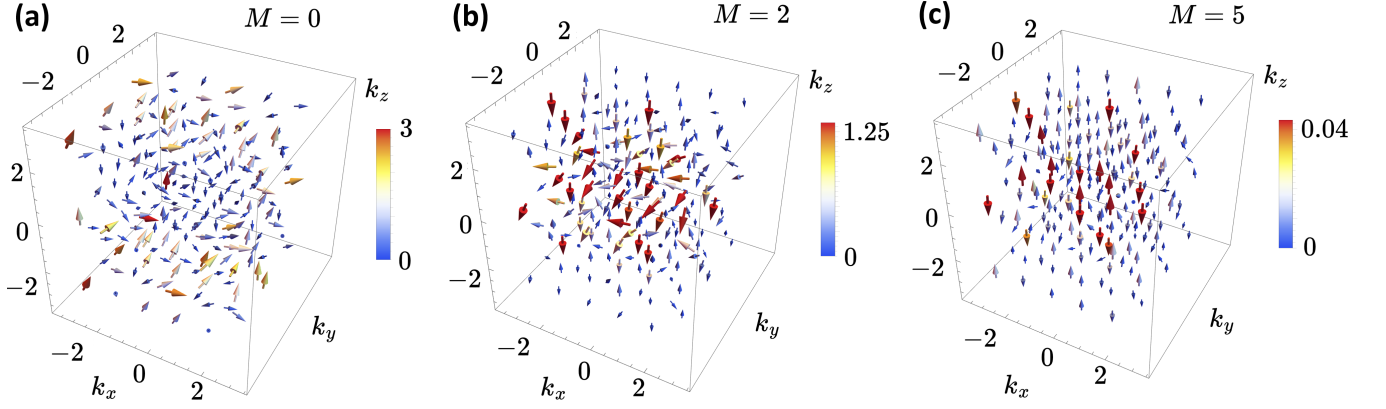


FIG. 4. Momentum space fields of the torsion tensor components, represented as vectors $(T_{xyz}, T_{yzx}, T_{zxy})$ over the 3D BZ $\cong T^3$. We choose the RHI model studied for the quantized shift effect in the main text, with topological mass M as a free parameter, and $w = 1$. (a) Setting $M = 0$ yields Hopf indices $(\chi_z, \chi_w) = (0, 2w)$, which is reflected by the high magnitudes of the torsion tensor components, (b) Crossing the TPT at $M = 3/2$ reduces the Hopf indices to $(\chi_z, \chi_w) = (0, -w)$, and the torsion tensor components individually decrease, yielding a reduced quantized circular shift effect on summation. (c) $M = 5$ trivializes the indices to $(\chi_z, \chi_w) = (0, 0)$, almost completely removing the torsion tensor components. The leftover values of $T_{xyz}, T_{yzx}, T_{zxy}$ cancel on performing a full summation over the BZ, yielding a vanishing effect quantized by the Hopf indices.

On summing all the terms and simplifying, using $A_{ij}^a = -A_{ji}^a$:

$$\begin{aligned} \sum_{m,n} (T_{abc}^{mn} + T_{bca}^{mn} + T_{cab}^{mn}) &= -2A_{12}^a (A_{13}^b A_{32}^c - A_{13}^c A_{32}^b) + \\ &-2A_{12}^b (A_{13}^c A_{32}^a - A_{13}^a A_{32}^c) - 2A_{12}^c (A_{13}^a A_{32}^b - A_{13}^b A_{32}^a). \end{aligned} \quad (\text{D13})$$

In terms of the two-band Euler connection: $\text{Eu}_{nm}^{ab} = \langle \partial_a u_n | \partial_b u_m \rangle - \langle \partial_b u_n | \partial_a u_m \rangle = \sum_{n \neq p \neq m} A_{np}^a A_{pm}^b - A_{np}^b A_{pm}^a$. Hence:

$$\sum_{m,n} (T_{abc}^{mn} + T_{bca}^{mn} + T_{cab}^{mn}) = -2A_{12}^a \text{Eu}_{12}^{bc} - 2A_{12}^b \text{Eu}_{12}^{ca} - 2A_{12}^c \text{Eu}_{12}^{ab}. \quad (\text{D14})$$

On identifying $\mathbf{a}^v = \mathbf{A}_{21} = -\mathbf{A}_{12}$, and $(\mathbf{Eu}^v)_a = \epsilon_{abc} \text{Eu}_{12}^{bc}$, we retrieve:

$$\sum_{m,n} (T_{abc}^{mn} + T_{bca}^{mn} + T_{cab}^{mn}) = -2\mathbf{a}^v \cdot \mathbf{Eu}^v. \quad (\text{D15})$$

In terms of the differential forms:

$$\sum_{m,n} (T_{abc}^{mn} + T_{bca}^{mn} + T_{cab}^{mn}) dk_x \wedge dk_y \wedge dk_z = -2a^v \wedge \text{Eu}^v, \quad (\text{D16})$$

which is the 3-form integrated to find the possible quantization in the three-band case. However, contrary to the four-band case, the topology of three-band models in three spatial dimensions has not been studied extensively, as for the time being. In particular, in three dimensions, a partitioning of three real bands into 2-band and 1-band subspaces can in principle yield a single \mathbb{Z} invariant, captured by the homotopy $\pi_3[\widetilde{\text{Gr}}_{1,3}(\mathbb{R})] \cong \pi_3[\text{SO}(3)/\text{SO}(2)] \cong \pi_3[S^2] \cong \mathbb{Z}$ associated with a single Hopf index [25]. We leave the exhaustive study of such topological phases, supporting the non-trivial real 3-form from Eq. (D16), as well as the torsional circular shift photoconductivity response, for future investigation.